Static polarizabilities of single-wall carbon nanotubes

Lorin X. Benedict, Steven G. Louie, and Marvin L. Cohen
Department of Physics, University of California at Berkeley, Berkeley, California 94720
and Materials Sciences Division, Lawrence Berkeley Laboratory, Berkeley, California 94720
(Received 7 December 1994)

The static electric polarizability tensor of single-wall carbon nanotubes is calculated within the random-phase approximation using a simple tight-binding model and a classical correction to include local fields. We find that the polarizability for constant fields parallel to the cylindrical axis is highly dependent on the details of the tube's electronic structure. In contrast, the polarizability for fields perpendicular to the axis only depends on the tube radius. The relative magnitudes of these two quantities suggests that under the application of a randomly oriented electric field, nanotubes acquire dipole moments pointing mainly along their axes, with the size of the dipole inversely proportional to the square of the minimum direct band gap.

I. INTRODUCTION

In this paper we examine the response of single-wall carbon nanotubes to a uniform external electric field $\mathbf{E}$. The main response of the electrons is the formation of an induced dipole moment $\mathbf{p}$. The quantity that relates the two is the polarizability tensor α, defined by $\mathbf{p} = \alpha\mathbf{E}$. Since the discovery of fullerenes, numerous investigations have been undertaken to determine $\alpha(\omega)$ and $\alpha(\omega = 0)$ for C_{60} both experimentally,[1] and theoretically.[2–4] Recently, calculations of the static polarizability have been done for many of the other stable clusters in the fullerene family as well.[5]

For the quasispherical fullerenes, there are two major contributions to $\alpha(\omega)$. There are the noninteracting single-particle excitations, which give rise to the noninteracting, or unscreened polarizability, α_0. This is defined by

$$\mathbf{p} = \alpha_0\mathbf{E}_{\mathrm{tot}}, \tag{1}$$

where $\mathbf{E}_{\mathrm{tot}}$ is the total electric field felt by the electrons. The polarizability α_0 can be calculated by perturbation theory with a knowledge of the single-particle energy levels and wave functions. The second contribution arises from the interaction between single-particle excitations, making $\mathbf{E}_{\mathrm{tot}}$ different from the externally applied field $\mathbf{E}$. It is the interacting, or screened polarizability defined by

$$\mathbf{p} = \alpha\mathbf{E} \tag{2}$$

that is the experimentally accessible quantity. For C_{60}, α_0 is roughly four times greater than α. This reflects the fact that $\mathbf{E}_{\mathrm{loc}} = \mathbf{E}_{\mathrm{tot}} - \mathbf{E}$ is large, due to the buildup of charge on the spherical surface containing the ions.[2]

In 1991, concentric carbon nanotubes were found,[6] and in 1992 single-wall tubes were first produced.[7] These can be thought of as the cylindrical analogues of the fullerene clusters, with the additional feature that the ideal infinite length structures are quasi-one-dimensional solids. The issue of the response of the tubes to electric fields is only beginning to be addressed. Random-phase approximation (RPA) calculations of $\epsilon(\mathbf{q}, \omega)$ have been done for electrons moving freely on a cylindrical surface.[8] Although these studies give qualitative insight into the positions of the zeros in $\epsilon(\mathbf{q}, \omega)$, they are unable to take into account the effects arising from the nanotube electronic structure. The most important electronic feature is the existence of an energy gap in most tubes. The size of the gap can drastically affect the magnitude and overall behavior of response functions. This becomes particularly important when coupled with the fact that tubes with roughly the same radius can have very different band gaps.[9,10] Cylindrical empty lattice calculations are unable to resolve these differences.

In this study, we address these issues by performing calculations which include the atomic structure of the carbon nanotubes. For simplicity, we focus on the $\mathbf{q} = 0$, $\omega = 0$ limit in an effort to understand the response to a static, uniform $\mathbf{E}$ field. The polarizability per unit length of single nanotubes is calculated, instead of a dielectric constant, in order to draw comparisons with the polarizabilities of fullerene clusters. The most obvious difference between nanotubes and spherical fullerenes is their cylindrical structure. This causes the α_0 and α of Eqs. (1) and (2) to be highly anisotropic tensors with principle axes $\hat{\mathbf{z}}$ (parallel to the cylindrical axis) and $\hat{\mathbf{x}}$ (perpendicular to the cylindrical axis). Using a tight-binding model, we will show that α_{0zz} is roughly proportional to $\frac{R}{E_g^2}$, where E_g is the minimum direct band gap and R is the tube radius, while α_{0xx} is independent of E_g and is just proportional to R^2. Arguments analogous to those used for C_{60} (Refs. 2 and 11) are then applied which relate α_0 to α. We find that even for insulating tubes, α_{zz} is an order of magnitude larger than α_{xx}. This implies that an external field with equal z and x components will give rise to a dipole moment pointing mainly along the z direction.

The structure of the paper is as follows. Section II contains the details of the models used. First the tight-binding theory of α_0 is presented, and then the classical

electrostatic model relating α_0 to α. Section III is a presentation of the results of the calculations for all of the tubes studied. Section IV provides an explanation of the findings. We conclude in Sec. V.

II. MODELS

A. Tight-binding model of α_0

Our tight-binding model for α_0 is based on the Ehrenreich-Cohen formalism for the dielectric function of a crystalline solid.[12] In this approach, $\epsilon(\mathbf{q},\omega)$ is calculated within the RPA using Bloch states as the basis. If we neglect local field effects, the real part of the dielectric function is given by

$$\epsilon_1(\mathbf{q},\omega) = 1 + 2\frac{4\pi e^2}{q^2\Omega}\sum_{\mathbf{k},n_1,n_2}\frac{|\langle \mathbf{k},n_1|e^{-i\mathbf{q}\cdot\mathbf{r}}|\mathbf{k}+\mathbf{q},n_2\rangle|^2}{E_{n_1}(\mathbf{k}) - E_{n_2}(\mathbf{k}+\mathbf{q}) - \hbar\omega} \times [f^0_{n_2}(\mathbf{k}+\mathbf{q}) - f^0_{n_1}(\mathbf{k})], \quad (3)$$

where $\mathbf{q}$ is restricted to the first Brillouin zone (the factor of 2 is for spin). In order to invoke the tight-binding approximations, we express the Bloch states in terms of localized atomiclike orbitals:

$$|\mathbf{k},n_1\rangle = \sum_\mu C_\mu(\mathbf{k},n_1) \times \left(\frac{1}{\sqrt{N}}\sum_{\mathbf{R}'} e^{i\mathbf{k}\cdot\mathbf{R}'}|\phi_\mu(\mathbf{r}-\tau_\mu-\mathbf{R}')\rangle\right), \quad (4)$$

$$|\mathbf{k}+\mathbf{q},n_2\rangle = \sum_\nu C_\nu(\mathbf{k}+\mathbf{q},n_2) \times \left(\frac{1}{\sqrt{N}}\sum_{\mathbf{R}} e^{i(\mathbf{k}+\mathbf{q})\cdot\mathbf{R}}|\phi_\nu(\mathbf{r}-\tau_\nu-\mathbf{R})\rangle\right), \quad (5)$$

where $\phi_\mu(\mathbf{r})$ and $\phi_\nu(\mathbf{r})$ are localized orbitals, τ_μ and τ_ν are vectors denoting the positions of the orbitals within a unit cell, and $\mathbf{R}'$ and $\mathbf{R}$ are the lattice translation vectors. C_μ and C_ν are the coefficients in the expansion of the Bloch states in terms of the ϕ_μ and ϕ_ν Bloch sums. We may now form the matrix element that enters the Ehrenreich-Cohen formula. Setting $\mathbf{R}' = 0$ and multiplying by N, we have

$$\langle \mathbf{k},n_1|e^{-i\mathbf{q}\cdot\mathbf{r}}|\mathbf{k}+\mathbf{q},n_2\rangle = \sum_{\mu\nu\mathbf{R}} C^*_\mu(\mathbf{k},n_1)C_\nu(\mathbf{k}+\mathbf{q},n_2)e^{i[(\mathbf{k}+\mathbf{q})\cdot\mathbf{R}-\mathbf{q}\cdot\tau_\mu]}\langle\phi_\mu(\mathbf{r})|e^{-i\mathbf{q}\cdot\mathbf{r}}|\phi_\nu(\mathbf{r}-\mathbf{d})\rangle, \quad (6)$$

where $\mathbf{d} = \tau_\nu - \tau_\mu + \mathbf{R}$.

Eventually, we will be interested in the $\mathbf{q}\to 0$ limit. Because $\phi_\mu(\mathbf{r})$ and $\phi_\nu(\mathbf{r})$ are localized, we may expand the matrix element in the right-hand side of Eq. (6) to first order in $\mathbf{q}\cdot\mathbf{r}$, obtaining

$$\lim_{\mathbf{q}\to 0}\langle\phi_\mu(\mathbf{r})|e^{-i\mathbf{q}\cdot\mathbf{r}}|\phi_\nu(\mathbf{r}-\mathbf{d})\rangle = \langle\phi_\mu(\mathbf{r})|\phi_\nu(\mathbf{r}-\mathbf{d})\rangle - i\langle\phi_\mu(\mathbf{r})|\mathbf{q}\cdot\mathbf{r}|\phi_\nu(\mathbf{r}-\mathbf{d})\rangle. \quad (7)$$

Here we choose to work within orthogonal tight binding; two localized orbitals have zero overlap unless they are equivalent, and are on the same site. Equation (7) then becomes

$$\lim_{\mathbf{q}\to 0}\langle\phi_\mu(\mathbf{r})|e^{-i\mathbf{q}\cdot\mathbf{r}}|\phi_\nu(\mathbf{r}-\mathbf{d})\rangle = \delta_{\mu\nu}\delta_{\mathbf{R}0} - i\mathbf{q}\cdot\mathbf{R}_{\mu\nu}(\mathbf{d}). \quad (8)$$

$\mathbf{R}_{\mu\nu}(\mathbf{d})$ is defined to be the matrix element of the operator $\mathbf{r}$ between ϕ_μ centered at the origin, and ϕ_ν centered at the position $\mathbf{d}$. We now have

$$\langle \mathbf{k},n_1|e^{-i\mathbf{q}\cdot\mathbf{r}}|\mathbf{k}+\mathbf{q},n_2\rangle \approx \sum_{\mu\nu\mathbf{R}} C^*_\mu(\mathbf{k},n_1)C_\nu(\mathbf{k}+\mathbf{q},n_2) \times e^{i[(\mathbf{k}+\mathbf{q})\cdot\mathbf{R}-\mathbf{q}\cdot\tau_\mu]} \times \left(\delta_{\mu\nu}\delta_{\mathbf{R}0} - i\mathbf{q}\cdot\mathbf{R}_{\mu\nu}(\mathbf{d})\right) \quad (9)$$

for $\frac{1}{|\mathbf{q}|}$ much greater than the characteristic unit cell length. Thus, we see that the matrix element is comprised of two terms. The first arises from the product of δ functions and will be referred to as the "δ term." It is equal to $\sum_\mu C^*_\mu(\mathbf{k},n_1)C_\mu(\mathbf{k}+\mathbf{q},n_2)e^{-i\mathbf{q}\cdot\tau_\mu}$. If there is only one atom per unit cell, or if $\mathbf{q}\cdot\tau_\mu = 0$ for all μ, this term is equal to zero. The second term depends on the dipole matrix elements $\mathbf{R}_{\mu\nu}(\mathbf{d})$ and will be called the "dipole term." Note that although the dipole matrix elements are multiplied by $\mathbf{q}$, both terms are the same order in $\mathbf{q}$ because of the $\mathbf{q}\cdot\tau_\mu$ term.

Unlike the quantities appearing in the δ term, the dipole matrix elements cannot be obtained as standard output from Slater-Koster tight-binding calculations. They must be input as external parameters. For the case of solids consisting solely of carbon, there are four localized orbitals in the tight-binding basis set used. They correspond to the carbon $2s$, $2p_x$, $2p_y$, and $2p_z$ states. At first sight, there are seven distinct dipole matrix elements, represented schematically in Fig. 1. One is on-site ($\mathbf{d} = 0$), while the others are off-site ($\mathbf{d} \neq 0$). (More precisely, there is a set of off-site dipole matrix elements for each order of nearest neighbors included.) These matrix elements are special because any $\mathbf{R}_{\mu\nu}(\mathbf{d})$ can be written as a linear combination of them, in a manner analogous to the Slater-Koster two-center integral formulas for Hamiltonian matrix elements.[13]

On closer inspection it is seen that the matrix elements

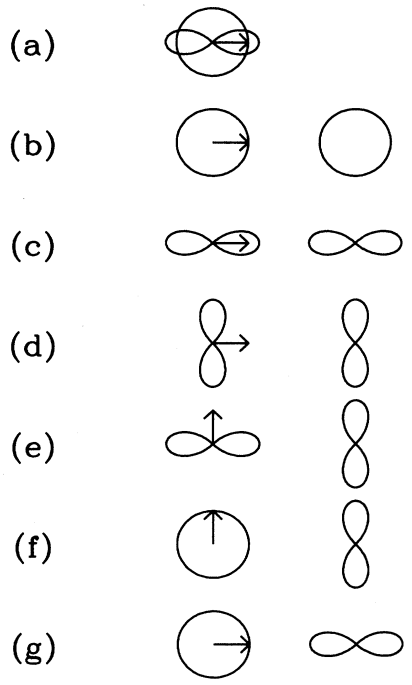

FIG. 1. Various dipole matrix elements between s and p atomiclike states. The first (a) is on-site, while the rest are off-site. The arrow indicates the direction of the vector $\mathbf{r}$, which gives a nonvanishing contribution to the matrix element.

denoted by d and e in Fig. 1 are actually equal, for $xp_y = yp_x$. Also, the assumption of orthogonal tight-binding forces b, c, and d to be zero. This is because the origin may be translated to the point $\frac{1}{2}\mathbf{d}$, where the integrals are zero by parity. Thus, we are left with three special dipole matrix elements, one on-site (a), and two off-site (f, g). Their magnitudes will be denoted R_{sp}, $R_{sp\pi}$, and $R_{sp\sigma}$, respectively.

The $\mathbf{R}_{\mu\nu}(\mathbf{d})$ must now be related to the special matrix elements. For the $\mathbf{d} = 0$ case, we have simply

$$\mathbf{R}_{sp_x}(0) = \mathbf{R}_{p_x s}(0) = R_{sp}\hat{\mathbf{x}}. \tag{10}$$

The off-site case is a bit more complicated. The relations can be derived by rotating the p orbital so that the axis of quantization is along $\mathbf{d}$. Let l, m, and n be the direction cosines of $\mathbf{d}$ with respect to x, y, and z, respectively. Then,

$$\begin{aligned}\mathbf{R}_{sp_x}(\mathbf{d}) &= \mathbf{R}_{p_x s}(\mathbf{d}) \\ &= [(1-l^2)R_{sp\pi} + l^2 R_{sp\sigma}]\hat{\mathbf{x}} \\ &\quad +[lm(R_{sp\sigma} - R_{sp\pi})]\hat{\mathbf{y}} \\ &\quad +[ln(R_{sp\sigma} - R_{sp\pi})]\hat{\mathbf{z}},\end{aligned} \tag{11}$$

$\mathbf{R}_{sp_y}$, and $\mathbf{R}_{sp_z}$ are obtained from Eqs. (10) and (11) by the cyclic permutations $x \to y \to z$, $l \to m \to n$. All other dipole matrix elements are zero within the framework of orthogonal tight binding. For simplicity, we limit the off-site matrix elements to include first nearest neighbors only. It is demonstrated below that this is not a serious restriction for the systems studied.

We define the unscreened polarizability per unit cell of a crystal by the relation

$$\lim_{\mathbf{q}\to 0} \epsilon_1(\mathbf{q},\omega) = 1 + \frac{4\pi}{\Omega}\alpha_0(\omega), \tag{12}$$

where $\epsilon_1(\mathbf{q},\omega)$ is given in Eq. (3). If there is no interaction between atoms in different unit cells, $\alpha_0(\omega)$ is just equal to the unscreened polarizability of the single molecule contained in each cell. Both ϵ_1 and α_0 are second-rank tensors. The individual components may be calculated by first determining the principle axes by symmetry, and then letting $\mathbf{q} \to 0$ along these directions. This yields the diagonal elements corresponding to each axis.

There are two sets of parameters that must be input into this model: Slater-Koster tight-binding parameters, which determine the energy eigenvalues and eigenstates, and dipole matrix elements. All carbon nanotubes are sp^2 bonded systems, so we use the first and second nearest neighbor Slater-Koster parameters of Tomanek and Louie.[14] These were originally designed to reproduce the band structure of graphite, and since have been applied successfully to the study of carbon nanotubes.[15] In order to determine the optimal values for R_{sp}, $R_{sp\sigma}$, and $R_{sp\pi}$, we must choose a reference system for which either ϵ_1 or α_0 is known. Because orthogonal tight-binding is used, it is desirable to choose a system that has a bonding configuration similar to that of the tubes. This will ensure the transferability of the parameters. C_{60} is a predominantly sp^2 bonded system with an experimentally determined screened polarizability. Unfortunately, our tight-binding model only has access to the unscreened polarizability. This has, however, been determined theoretically by Pederson and Quong[16] using *ab initio* local density functional theory. They obtained a result of 311 Å^3 per molecule for $\alpha_0(\omega = 0)$, roughly four times larger than the experimental value for the screened polarizability,[1] as expected. We have calculated $\alpha_0(\omega = 0)$ of C_{60} using our model for a wide range of different R_{sp}, $R_{sp\sigma}$, and $R_{sp\pi}$. We find a sensitive dependence of $\alpha_0(\omega = 0)$ on R_{sp}, whereas the dependence on the off-site matrix elements is negligible. Therefore, $R_{sp\sigma}$ and $R_{sp\pi}$ may be set equal to zero. The local density functional result is then obtained if $R_{sp} = 0.5$ Å. If $R_{sp\sigma}$ and $R_{sp\pi}$ are changed, the value of $\alpha_0(\omega = 0)$ is only slightly altered. For instance, if $R_{sp\sigma}$ and $R_{sp\pi}$ are both set equal to 0.5 Å while keeping $R_{sp} = 0.5$ Å, $\alpha_0(\omega = 0)$ is changed by less than 5%.

We have therefore constructed a tight-binding model of the $\mathbf{q} = 0$ dielectric response function without local field effects for sp^2 bonded carbon systems, in which the only external parameter is an on-site $s-p$ dipole matrix element. Before the issue of local fields is addressed, two points must be made: (1) The value of $R_{sp} = 0.5$ Å is not to be understood as the dipole matrix element between true atomic carbon $2s$ and $2p$ wave functions. As stated above, the localized orbitals of this model are orthogonalized orbitals that may be very different from their atomic counterparts. (2) The parameters of the model

have been chosen to describe sp^2 bonded systems. If we wish to study systems with other bonding configurations, both the Slater-Koster parameters, and the dipole matrix elements may need to be changed.

B. Local field correction: Relating α_0 to α

The difference between the unscreened polarizability α_0, defined in Eq. (1), and the screened polarizability α of Eq. (2) is due to the difference between the total and applied electric fields. This arises because the virtual single-particle excitations have electric charge, and produce a local field. Stated another way, α_0 only accounts for the polarization of the individual single-particle wave functions, while α includes their mutual interaction as well. For most bulk crystals, local field effects change ϵ by roughly 10%.[17] For surfaces, however, the effect is much greater due to the buildup of bound surface charge. Since fullerenes are closed surfaces, local field effects are large. This is the reason for the factor of 4 difference between α_0 and α of C_{60}.

Local fields can be taken into account within RPA by considering charge fluctuations inside a unit cell, i.e., $\mathbf{q}$ of Eq. (3) outside the first Brillouin zone. From the previous section, we see that our tight-binding model is only valid for $\mathbf{q} \to 0$. Thus, a straightforward application of RPA is not possible here. Instead we can take advantage of the simple geometries of fullerenes, and construct classical models that relate $\mathbf{E}$ to $\mathbf{E}_{\text{tot}}$. This determines the relationship between α_0 and α via Eqs. (1) and (2). The simplest possible model is one in which the local field, $\mathbf{E}_{\text{loc}} = \mathbf{E}_{\text{tot}} - \mathbf{E}$, is constant within the fullerene. This is reasonable if the fullerene is ellipsoidal.[18]

As an example, consider C_{60}.[2,11] If a spatially constant external field $\mathbf{E}$ is applied, bound charge will form at the surface of the sphere. This will create a depolarization field $\mathbf{E}_{\text{loc}}$ pointing opposite to $\mathbf{E}$. If we assume that this field is constant within the sphere, then $\mathbf{E}_{\text{tot}}$ will be constant inside as well. We can relate the magnitude of this field to the induced dipole moment, $E_{\text{loc}} = \frac{p}{R^3}$. Equations (1) and (2) then give us the relationship between α_0 and α:

$$\alpha(\omega) = \frac{\alpha_0(\omega)}{1 + \frac{\alpha_0(\omega)}{R^3}}. \tag{13}$$

We see that α is less than α_0, as expected. However, the maximum value of α is $R^3 = 45$ Å^3. This is inconsistent with the experimental result of 80 Å^3.[1,11] The discrepancy can be understood by noting that the electrons that participate in the screening are not confined to the sphere containing the ions. This can be taken into account with a single parameter, δR, such that the "effective radius" is $R_{\text{eff}} = R + \delta R$,[11]

$$\alpha(\omega) = \frac{\alpha_0(\omega)}{1 + \frac{\alpha_0(\omega)}{R_{\text{eff}}^3}}. \tag{14}$$

If we take the local density functional theory value of 311 Å^3 for α_0, the experimental value of α is reproduced when $\delta R = 1.2$ Å.

The same arguments will now be applied to single-wall carbon nanotubes. Again, the goal will be to relate $\mathbf{E}$ to $\mathbf{E}_{\text{tot}}$ in order to determine the relationship between α_0 and α. The crucial difference between nanotubes and C_{60} is their cylindrical structure. If $\mathbf{E}$ is in the $\hat{\mathbf{x}}$ direction, bound charge will build up on the surface and create a local depolarization field. If $\mathbf{E}$ is along $\hat{\mathbf{z}}$, there will be no bound surface charge, so $\mathbf{E}_{\text{loc}} = 0$ within this model. This is, of course, only true in the ideal case of an infinitely long tube. For a tube of finite length, an external field in the $\hat{\mathbf{z}}$ direction will induce bound charge at the ends. However, the resulting local field will be negligible as long as the length is much larger than the diameter. Thus, we will assume that $\mathbf{E}_{\text{loc}}$ has no z component.

Since the principle axes of α_0 and α are $\hat{\mathbf{z}}$ and $\hat{\mathbf{x}}$ (see below), we need only consider the two cases of $\mathbf{E}$ along these directions. Let $\mathbf{E}$ be along $\hat{\mathbf{x}}$ ($\perp \hat{\mathbf{z}}$). There will then be a local field in the x direction. Assume that it is constant inside the tube. The surface charge density per length, which gives rise to a constant field along $\hat{\mathbf{x}}$, is of the form $\sigma(\phi) = \sigma_0 \cos\phi$, where ϕ is the azimuthal angle measured with respect to $\hat{\mathbf{x}}$. The resulting dipole moment per length is

$$\begin{aligned} p_x &= R \int d\phi x \sigma(\phi) \\ &= 2R \int_0^{\pi} d\phi R \cos\phi \sigma_0 \cos\phi = \pi R^2 \sigma_0. \end{aligned} \tag{15}$$

With this and Eq. (1), we have

$$\sigma(\phi) = \frac{p_x}{\pi R^2} \cos\phi = \frac{\alpha_{0xx} E_{\text{tot}x}}{\pi R^2} \cos\phi, \tag{16}$$

where σ, p, and α are all defined per unit length. We can now calculate the local electric field due to $\sigma(\phi)$. It can be shown to be constant within the tube and equal to

$$\mathbf{E}_{\text{loc}} = -\frac{2\alpha_{0xx} E_{\text{tot}x}}{R^2} \hat{\mathbf{x}}. \tag{17}$$

Knowing that $\mathbf{E}_{\text{tot}} = \mathbf{E} + \mathbf{E}_{\text{loc}}$, we may use Eqs. (1), (2), and (17) to obtain

$$\alpha_{xx} = \frac{\alpha_{0xx}}{1 + 2\frac{\alpha_{0xx}}{R^2}}. \tag{18}$$

If $\mathbf{E}$ is along $\hat{\mathbf{z}}$, then $\mathbf{E}_{\text{loc}} = 0$. This means that $\mathbf{E}_{\text{tot}} = \mathbf{E}$ and we get simply

$$\alpha_{zz} = \alpha_{0zz}. \tag{19}$$

Note that all polarizabilities are defined per unit length.

If we combine Eqs. (18) and (19) and restore the frequency dependance, we can write $\alpha(\omega)$ as a matrix

$$\alpha(\omega) = \begin{pmatrix} \frac{\alpha_{0xx}(\omega)}{1 + 2\frac{\alpha_{0xx}(\omega)}{R^2}} & 0 \\ 0 & \alpha_{0zz}(\omega) \end{pmatrix}. \tag{20}$$

It should be pointed out that α is actually a 3×3 ma-

trix, for $\hat{\mathbf{x}}$ can lie anywhere in the plane perpendicular to $\hat{\mathbf{z}}$. Since all x axes are equivalent, we suppress one dimension. As for C_{60}, $\alpha_{xx} < \alpha_{0xx}$; Eq. (18) is the two-dimensional analogue of Eq. (13). Likewise, we anticipate that it will be necessary to replace R by $R_{\text{eff}} = R + \delta R$. The question of what is the appropriate δR is not a simple one. However, we expect the magnitude of δR to reflect the intrinsic features of π systems, such as the extent of a p orbital, etc. Thus, we fix $\delta R = 1.2$ Å as for C_{60}. We show below that the results are not sensitive to this choice.

The most important feature of Eq. (20) is that α_{zz} remains unscreened. This has two interesting consequences: (1) Even if α_{0xx} and α_{0zz} are comparable, α_{zz} will be significantly greater than α_{xx}. This means that an external electric field with equal z and x components will give rise to an electric dipole moment pointing primarily along $\hat{\mathbf{z}}$. (2) The response of the tubes to electric fields will be particularly sensitive to the details of the tube electronic structure. As we stated above, α_0 is determined from the single-particle energies and eigenstates [Eq. (3)]. If the energy gap is small, α_{0zz} may be quite large. Because of Eq. (19), α_{zz} will be large as well. This is not true for the caged fullerenes, in which all components of the polarizability tensor are governed by expressions like Eq. (14); as long as α_0 is large enough, α is completely determined by $R_{\text{eff}} \sim R$. *The absence of a large screening field along the axes of the tubes makes it necessary to consider band structure effects in these systems.*

We are now in a position to calculate $\alpha(\omega = 0)$ for a wide range of tubes. Our strategy is simple. First, a tight-binding calculation is performed to determine the $E_n(\mathbf{k})$, and $C_\mu(\mathbf{k}, n)$ appearing in Eqs. (3) and (9). Then a small $\mathbf{q}$ is chosen along $\hat{\mathbf{z}}$. $\epsilon_1(\mathbf{q}, \omega = 0)$ without local fields is calculated using Eqs. (3), (9), and (10), and $R_{sp} = 0.5$ Å ($R_{sp\sigma} = R_{sp\pi} \equiv 0$). Smaller and smaller $\mathbf{q}$ are chosen, and $\lim_{\mathbf{q}\to 0} \epsilon_1(\mathbf{q}, \omega = 0)$ is obtained. We then choose $\mathbf{q}$ along $\hat{\mathbf{x}}$ and repeat the procedure. The $\alpha_0(\omega = 0)$ tensor is calculated using Eq. (12). Finally, we use the electrostatic model of Eq. (20) with R replaced by $R_{\text{eff}} = R + 1.2$ Å to determine the $\alpha(\omega = 0)$ tensor. Results of these calculations are presented for tubes having a variety of different radii and band gaps in the next section.

III. RESULTS

We consider ideal infinitely long tubes that are obtained by rolling a graphite sheet around a cylinder. The (n_1, n_2) notation of Saito *et al.*[10] will be used throughout. Here, each tube is identified by its circumference vector $\mathbf{c} = n_1\mathbf{a}_1 + n_2\mathbf{a}_2$, where $\mathbf{a}_1$ and $\mathbf{a}_2$ are primitive translation vectors of the graphite sheet, which are chosen to be 60° apart. All (n, n) tubes are metallic, while others are semiconductors. If $n_1 - n_2$ is a nonzero multiple of three, the tube is a very small gap semiconductor.[9] There is a general reduction of the band gaps as the radii increase. This is because the infinite radius case is identical to a planar graphite sheet, which is a semimetal.

Before results are presented, it is worth considering the criteria on n_1 and n_2 such that the (n_1, n_2) tube has the symmetry required by Eq. (20). We have assumed above that $\hat{\mathbf{x}}$ and $\hat{\mathbf{z}}$ are principle axes of the α_0 and α tensors. It can be shown that any second-rank symmetric tensor in three dimensions is "isotropic" in a plane perpendicular to a three- or morefold axis of rotation;[18] i.e., every direction perpendicular to the rotation axis is a principle axis. Thus, all tubes of the form $(n, 0)$ and (n, n) with $n \geq 3$ have the required symmetry. The same statement is true for screw axes. Therefore, all (n_1, n_2) tubes with $n_1 \neq n_2$ are included as well. This set comprises all tubes of interest, for the ones not included are probably too small to ever be found. In what follows, we may refer to the direction $\hat{\mathbf{x}}$ without specifying where it is pointing with respect to the individual atoms.[19]

We have calculated the static unscreened and screened polarizabilities of the $(n, 0)$ tubes for $9 \leq n \leq 19$. The (n, n) tubes (4,4), (5,5), and (6,6) have also been studied, as well as the chiral tubes (4,2) and (5,2). Table I contains a list of the results. Since $\alpha_{0zz} = \alpha_{zz}$, only α_{zz} is shown. In the cases where $n_1 - n_2$ is a multiple of three, the minimum band gap is very small (or zero), and α_{zz} is effectively infinite. Thus, we choose not to list it here. Note that this is not true for α_{0xx}. This will be discussed at length below.

The first issue to be addressed is the overall magnitude of the polarizabilities. If we multiply each value by a length, and divide by the number of carbon atoms per that length, we obtain the polarizabilities per atom (Å^3). We may compare these to the polarizabilities per atom of fullerene clusters. Because tubes are cylinders and the clusters are quasispherical, their local field contributions are quite different. Therefore, it is only meaningful to compare the unscreened polarizabilities. The quantity that is most analogous to α_0 of C_{60} is α_{0xx}. Its value increases monotonically with R. It is 3.8 Å^3/atom for the (4,2) tube, and 8.5 Å^3/atom for (19,0). This

TABLE I. Static polarizabilities per unit length (in Å^2) of various carbon nanotubes of radius R (Å). In cases where $n_1 - n_2$ is a multiple of three, α_{zz} is extremely large and is not given.

Tube (n_1, n_2)	R	α_{zz}	α_{0xx}	α_{xx}
(9,0)	3.57		40.6	8.9
(10,0)	3.94	174.7	48.5	10.3
(11,0)	4.33	171.6	57.8	12.1
(12,0)	4.73		65.7	13.9
(13,0)	5.12	292.4	76.1	15.8
(14,0)	5.52	268.3	87.4	17.9
(15,0)	5.91		97.4	20.1
(16,0)	6.30	445.5	109.9	22.4
(17,0)	6.70	401.4	123.6	24.9
(18,0)	7.09		136.3	27.4
(19,0)	7.49	651.1	150.6	30.2
(4,4)	2.73		26.6	6.0
(5,5)	3.41		37.4	8.3
(6,6)	4.10		49.8	11.0
(4,2)	2.09	49.1	18.8	4.2
(5,2)	2.46		23.1	5.2

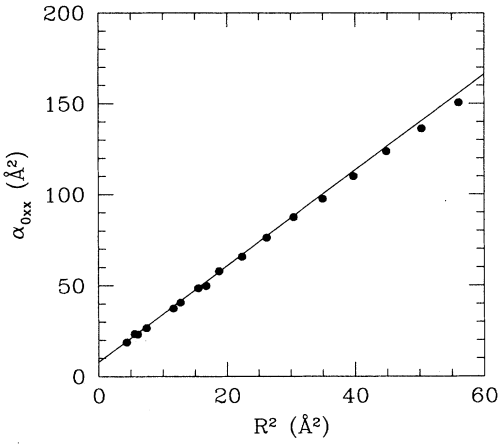

FIG. 2. Plot of α_{0xx} vs R^2 for the tubes studied. The solid line is a linear least squares fit to the points.

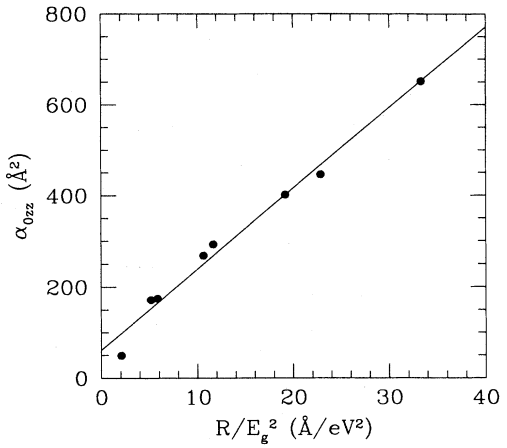

FIG. 3. Plot of α_{0zz} $(= \alpha_{zz})$ vs $\frac{R}{E_g^2}$ for the (n_1, n_2) tubes studied where $n_1 - n_2$ is *not* equal to an integer multiple of three. A linear least squares fit is also shown.

is consistent with the C_{60} value of roughly 5 Å^3/atom. The general increase with radius is also consistent with a similar trend in fullerene clusters[5] if we assume that α is a monotonically increasing function of α_0, as in Eq. (14). We see that α_{0zz} is considerably larger than α_{0xx}. This is a result of the anisotropy of the single-particle wave functions (i.e., graphite is more polarizable along the sheet plane direction than in the perpendicular direction). It manifests itself in the matrix elements of Eq. (3).

The increase of α_{0xx} with radius can be quantified by plotting α_{0xx} versus R^2, as shown in Fig. 2. We see that α_{0xx} is roughly proportional to R^2 with a slope of 2.6, independent of the tube chirality and band gap. Even the zero gap (n, n) tubes have finite α_{0xx}, and obey this simple relation. The fact that α_{0xx} is completely independent of the minimum band gap is particularly striking. It suggests that there are selection rules that force the matrix elements of Eq. (3) to be zero in cases where the energy denominator is small. We will explore the origin of these selection rules in the next section.

Unlike α_{0xx}, α_{0zz} $(= \alpha_{zz}$ in the present theoretical framework) is highly dependent on the minimum gap. In cases where the gap is zero, α_{0zz} is infinite. This means that the above selection rules for the matrix elements do not apply when $\mathbf{q}$ is in the z direction. There is also a dependence of this quantity on the tube radius. In fact, α_{0zz} is approximately linear in $\frac{R}{E_g^2}$, as shown in Fig. 3. An explanation of this behavior is given in the following section.

As can be seen from Table I, $\alpha_{xx} \sim \frac{1}{5}\alpha_{0xx}$ for each tube. This is a consequence of Eq. (18), with R replaced by $R + \delta R = R + 1.2$ Å. These results are relatively insensitive to the choice of δR; a factor of 2 increase or decrease in δR changes α_{xx} by no more than 40%. The ratio $\frac{\alpha_{zz}}{\alpha_{xx}}$ is > 11 for all tubes studied. For very small gap tubes, the ratio is extremely large. This, along with Eq. (2), justifies our prediction that an external electric field with equal z and x components will give rise to a dipole moment pointing mainly along $\hat{\mathbf{z}}$. Likewise, the magnitude of this dipole moment will depend mostly on α_{zz} and will therefore be roughly proportional to $\frac{R}{E_g^2}$. It should be understood that the relationship implied by Eq. (18) is approximate. More sophisticated models for local field effects may yield results different from those presented here. However, we expect the general features to be correct.

IV. DISCUSSION

In this section, we explore the origins of the dependence of α_{0xx} and α_{0zz} on R and E_g. First, we see why α_{0xx} is independent of the minimum gap. Then its proportionality to R^2 is explained using an empty lattice model. Finally, the linear variation of α_{0zz} with $\frac{R}{E_g^2}$ is understood from the point of view of a simple model based on the oscillator strength sum rule.

In order for α_{0xx} to be completely independent of the minimum gap, the matrix elements of Eq. (3) must be zero when the energy denominator has its smallest values. We can see that this is true by examining the quantity $\langle \mathbf{k}, n_1 | e^{-i\mathbf{q}\cdot\mathbf{r}} | \mathbf{k}+\mathbf{q}, n_2 \rangle$ when $\mathbf{q} = q\hat{\mathbf{x}}$. Since we are considering individual tubes, the states $|\mathbf{k}, n_1\rangle$ and $|\mathbf{k}+\mathbf{q}, n_2\rangle$ are localized along the directions perpendicular to $\hat{\mathbf{z}}$. The matrix element may then be expanded to first order in $\mathbf{q}\cdot\mathbf{r}$ $(= qx)$. Also, the absence of dispersion in the x direction allows us to write $|\mathbf{k}+\mathbf{q}, n_2\rangle = |\mathbf{k}, n_2\rangle$. This yields

$$\begin{aligned}\lim_{\mathbf{q}\to 0} \langle \mathbf{k}, n_1 | e^{-i\mathbf{q}\cdot\mathbf{r}} | \mathbf{k}+\mathbf{q}, n_2 \rangle &= \langle \mathbf{k}, n_1 | \mathbf{k}, n_2 \rangle \\ &\quad - i \langle \mathbf{k}, n_1 | \mathbf{q}\cdot\mathbf{r} | \mathbf{k}, n_2 \rangle \\ &= -iq \langle \mathbf{k}, n_1 | \hat{\mathbf{x}}\cdot\mathbf{r} | \mathbf{k}, n_2 \rangle \quad (21)\end{aligned}$$

for $n_1 \neq n_2$. As discussed by previous workers,[9,10] the Bloch states of nanotubes arise from lines of allowed k vectors of the graphite sheet Brillouin zone which point along $\hat{\mathbf{k}}_z$. In the Appendix, we use group theory to show that $\langle \mathbf{k}, n_1 | \hat{\mathbf{x}}\cdot\mathbf{r} | \mathbf{k}, n_2 \rangle = 0$ if $|n_1\rangle$ and $|n_2\rangle$ arise from the

same line, as long as it is *not* the line that is farthest from Γ in $(n,0)$ and (n,n) tubes with odd n. In the absence of strong $\sigma-\pi$ hybridization,[15] the minimum direct gap is always between states coming from the same line. This line intersects Γ for the case of (n,n) tubes, and is not the line farthest from Γ in $(n,0)$ tubes unless $n<5$. This means that $\langle \mathbf{k},n_1|e^{-iq\hat{\mathbf{x}}\cdot\mathbf{r}}|\mathbf{k}+q\hat{\mathbf{x}},n_2\rangle$ is zero between highest occupied molecular orbital (HOMO) and lowest occupied molecular orbital (LUMO) states of all chiral tubes, (n,n) tubes, and $(n,0)$ tubes with $R>2.0$ Å. Thus, it follows that α_{0xx} is independent of the HOMO and LUMO states and hence E_g in these cases.

The fact that α_{0xx} is approximately proportional to R^2 can be best understood by appealing to an empty lattice model of electrons moving freely on a cylinder of infinitesimal thickness. Such a model has been used by several authors to study collective modes of nanotubes.[8] In this approach, the π-electron Bloch states of a tube of radius R may be written as $\langle \mathbf{r}|k,n\rangle=\frac{1}{2\pi\sqrt{R}}e^{ikz}e^{in\phi}$, where n is an integer. Their energies are $E_n(k)=\frac{\hbar^2}{2m^*}\left[\left(\frac{n}{R}\right)^2+k^2\right]$. The band index n now refers to the rotational subbands of the π-electron complex, which arise from the lines of allowed k vectors mentioned above. Each one of these bands will be folded back in a reduced zone scheme, and will acquire gaps at the Fermi energy with the addition of the crystalline potential. Therefore, every free-electron band corresponds to many bands of the tight-binding calculation. We choose to use an extended-zone scheme to simplify the argument that follows.

From the considerations outlined above, such as the absence of dispersion in the $\hat{\mathbf{x}}$ direction, we have

$$\alpha_{0xx}=e^2\int\frac{dk}{2\pi}\sum_{n_1,n_2}\frac{|\langle k,n_1|\hat{\mathbf{x}}\cdot\mathbf{r}|k,n_2\rangle|^2}{E_{n_1}(k)-E_{n_2}(k)}\times[f^0_{n_2}(k)-f^0_{n_1}(k)]. \tag{22}$$

The matrix elements of this expression can be shown to be independent of k and proportional to R. They are only nonzero if n_1 and n_2 differ by one. The energy denominator is equal to $\frac{\hbar^2}{2m^*R^2}({n_1}^2-{n_2}^2)$ independent of k. Thus,

$$\alpha_{0xx}\propto\int_0^{k_F}dk\sum_{n=0}^{\infty}\frac{R^2\frac{2m^*R^2}{\hbar^2}}{2n-1}[f^0_{n-1}(k)-f^0_n(k)], \tag{23}$$

k_F is the Fermi wave vector, equal to $\frac{\sqrt{2m^*E_F}}{\hbar}$. It is the wave vector where the $n=0$ band crosses E_F. Let k_n denote the k point where the nth band crosses E_F. We then have $\cdots<k_2<k_1<k_0=k_F$. Because of the difference of zero temperature Fermi factors, we are forced to set $n=j$ when $k\in[k_j,k_{j-1}]$. The integral can then be evaluated in piecewise fashion over the intervals $[k_n,k_{n-1}]$

$$\alpha_{0xx}\propto\frac{2m^*R^4}{\hbar^2}\sum_{n=0}^{n_F}\frac{k_{n-1}-k_n}{2n-1}. \tag{24}$$

n_F is the largest n such that $\frac{\hbar^2n^2}{2m^*R^2}<E_F$. The interval length $k_{n-1}-k_n=\sqrt{\frac{2m^*E_F}{\hbar^2}-\left(\frac{n-1}{R}\right)^2}-\sqrt{\frac{2m^*E_F}{\hbar^2}-\left(\frac{n}{R}\right)^2}$ may be approximated by

$$k_{n-1}-k_n\approx\frac{\hbar}{2\sqrt{2m^*E_F}R^2}(2n-1), \tag{25}$$

for $n\ll n_F$. These are the terms that contribute most to the sum. If we neglect the large n terms, Eqs. (24) and (25) yield the approximate relation

$$\alpha_{0xx}\propto\sqrt{\frac{m^*}{E_F}}R^2. \tag{26}$$

Since m^* and E_F are roughly independent of the tube size (for tubes large enough so that the zone-folding picture applies), $\alpha_{0xx}\propto R^2$ as expected. Therefore, we see that the behavior shown in Fig. 2 is due to three properties of the systems: (1) The matrix element of Eq. (21) is proportional to R, and is only nonzero when n_1 and n_2 correspond to rotational subbands that are adjacent in energy. (2) The energy difference between rotational subbands is proportional to $\frac{1}{R^2}$. (3) m^* and E_F are roughly independent of R. Although this discussion has involved a cylindrical shell empty lattice model, the conclusions are valid for nanotubes large enough so that hybridization effects do not play a dominant role.

We now turn to a discussion of α_{0zz}. For this case, we consider Eq. (3) with $\mathbf{q}=q\hat{\mathbf{z}}$. The relevant Bloch states are $\mathbf{q}$ dependent, and the matrix elements are of the form $\langle \mathbf{k},n_1|f(q,z)|\mathbf{k}+\mathbf{q},n_2\rangle$. Therefore, the above selection rules do not apply; the matrix elements between HOMO and LUMO bands are nonzero. Because the minimum gap in most tubes is small, we expect α_{0zz} to be dominated by terms for which the energy denominator is roughly equal to E_g. This makes it reasonable to assume that the linear dielectric response will be adequately described by a model in which all virtual single-particle transitions of a given tube have the same energy $\bar{E}_g$, which is of the order of E_g. A model of this type has been constructed for $\epsilon(\mathbf{q}=0,\omega=0)$ from a generalized Thomas-Rieche-Kuhn sum rule,[20]

$$\epsilon=1+\left(\frac{\hbar\omega_p}{\bar{E}_g}\right)^2, \tag{27}$$

where ω_p is the plasma frequency, equal to $\sqrt{\frac{4\pi e^2N_e}{\Omega m}}$, and N_e is the number of electrons per cell that participate in the screening. For this we use 4/atom, because one carbon $2s$ and three $2p$ electrons were considered in the RPA calculation. $\bar{E}_g$ is the "average gap" of the system. The approximate linearity in the separation of the π bands near the Fermi level suggests that $\bar{E}_g$ will vary linearly with E_g (since there is much less contribution from states far away from E_F).

If we use Eq. (12) to convert Eq. (27) into an expression involving α_{0zz}, we get

$$\alpha_{0zz}=\left[\frac{8\pi\hbar^2e^2}{mA}\right]\left(\frac{R}{\bar{E}_g{}^2}\right), \tag{28}$$

where A is the area per atom on the graphite sheet (again, α_{0zz} is defined per unit length). This establishes the linear dependence on $\frac{R}{\bar{E}_g^2}$ since we expect $\bar{E}_g \propto E_g$. We may use the plot of Fig. 3 to determine the precise relation between $\bar{E}_g$ and E_g. The least squares linear fit to the points has a slope of 17.8 eV^2 Å. This, along with Eq. (28), gives $\bar{E}_g \sim 5.4E_g$; a reasonable result considering that the HOMO and LUMO bands of tubes have large dispersion.

V. CONCLUSIONS

We have used a tight-binding model and a classical electrostatic argument to calculate the static polarizability of single-wall carbon nanotubes. It was shown that the polarizability tensor is highly anisotropic, a consequence of the inherent anisotropy of the tubes. The polarizability for external fields in the $\hat{\mathbf{z}}$ direction is considerably larger than that for fields along the $\hat{\mathbf{x}}$ direction. From this we conclude that a randomly oriented field will, on average, give rise to a dipole moment pointing mainly along the tube axis. The size of the moment is proportional to the tube radius divided by the square of the band gap. This may have significant consequences, for it suggests that tubes with different atomic arrangements respond very differently to external fields, even if the tube radii are similar. The issue of nonzero frequency, although not considered here, can be addressed easily within this model. One must only use a range of different ω in the denominator of Eq. (3). In addition, the calculated matrix elements and their associated selection rules can be used to compute the frequency dependent transverse dielectric function. This could provide a key to understanding the results of subsequent absorption measurements. The exotic geometric and electronic structures of carbon nanotubes could provide some unique dielectric responses.

ACKNOWLEDGMENTS

This work was supported by the National Science Foundation Grant No. DMR-9120269 and by the Director, Office of Energy Research, Office of Basic Energy Sciences, Materials Sciences Division of the U.S. Department of Energy under Contract No. DE-AC03-76SF-00098. We thank X. Blase, Dr. A. Rubio, and Dr. Y. Miyamoto for helpful discussions. In addition, L.X.B. extends much thanks to Dr. E. L. Shirley for his many helpful discussions and contributions during the early stages of this work.

APPENDIX

We wish to show that $\langle n_1|\hat{\mathbf{x}}\cdot\mathbf{r}|n_2\rangle = 0$ if $|n_1\rangle$ and $|n_2\rangle$ arise from the same line of allowed k vectors pointing along $\hat{\mathbf{k}}_z$. To do this, we must consider the symmetry groups of tubes. We first discuss the nonchiral $(n,0)$ and (n,n) tubes. They have symmorphic space groups, with the point subgroups C_{nv}.[21] C_{nv} consists of powers of C_n rotations and reflections. For n even, C_{nv} has $\frac{n}{2}+3$ irreducible representations labeled $A_1, A_2, B_1, B_2, E_1, E_2, ..., E_{\frac{n}{2}-1}$. A_1 is the totally symmetric representation. It has z as a basis function. (The z direction is defined to be the C_n axis.) For odd n, C_{nv} has the $\frac{n-1}{2}+2$ irreducible representations $A_1, A_2, E_1, E_2, ..., E_{\frac{n-1}{2}}$. Again, A_1 is the symmetric representation that has the symmetry of z. For both even and odd cases, E_1 has x and y as basis functions. The states $|n_1\rangle$ and $|n_2\rangle$ are eigenstates of the Hamiltonian, so they transform according to irreducible representations of the point group. The operator $\hat{\mathbf{x}}\cdot\mathbf{r}$ can also be classified according to symmetry. $\langle n_1|\hat{\mathbf{x}}\cdot\mathbf{r}|n_2\rangle$ will be zero if the combined symmetry does not contain the totally symmetric representation, i.e.,

$$\Gamma(|n_1\rangle)\times\Gamma(\hat{\mathbf{x}}\cdot\mathbf{r})\times\Gamma(|n_2\rangle) \not\supset A_1 \Longrightarrow \langle n_1|\hat{\mathbf{x}}\cdot\mathbf{r}|n_2\rangle = 0. \tag{A1}$$

Because $\hat{\mathbf{x}}\cdot\mathbf{r} = x$, $\Gamma(\hat{\mathbf{x}}\cdot\mathbf{r}) = E_1$. Thus,

$$\Gamma(|n_1\rangle)\times\Gamma(|n_2\rangle) \not\supset E_1 \Longrightarrow \langle n_1|\hat{\mathbf{x}}\cdot\mathbf{r}|n_2\rangle = 0. \tag{A2}$$

It can be shown that states that arise from particular lines transform according to specific irreducible representations of the point group. As an example, consider the $(4,4)$ tube. Its corresponding allowed lines are shown in Fig. 4 along with the symmetrical Brillouin zone of the graphite sheet. The dashed lines mark the boundary of the Brillouin zone of the $(1,1)$ unit. Each line

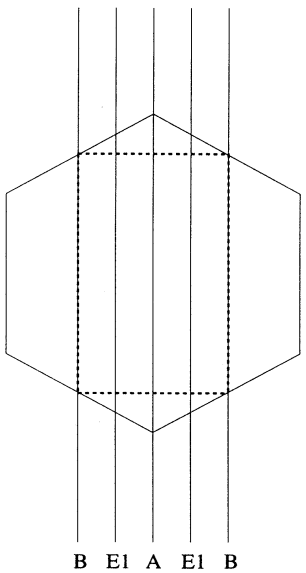

FIG. 4. Allowed k vectors of the $(4,4)$ tube mapped onto the graphite sheet Brillouin zone. The dashed lines enclose the Brillouin zone of a single $(1,1)$ unit. Each line is identified with irreducible representations of the point group C_{4v}. A denotes A_1, A_2 and B denotes B_1, B_2.

is associated with one or more irreducible representations of C_{4v}. The center line intersects the Γ point of the graphite sheet, and is associated with A_1 and A_2. The lines farthest from Γ are associated with B_1 and B_2. The two middle lines on either side of the center belong to E_1. Similar assignments can be made for all even n (n,n) tubes. It is always true that A_1, A_2 correspond to the center line and B_1, B_2 to the lines farthest out. $E_1, E_2, ..., E_j, ...$, are always between the two, with E_j being associated with the jth lines away from the center on both sides. The picture for odd n (n,n) tubes is the same, except that the lines farthest from Γ belong to $E_{\frac{n-1}{2}}$. For $(n,0)$ tubes, we must only rotate the hexagon by 90°, and change the density of the lines.[9] Everything else remains the same.

Assume that $|n_1\rangle$ and $|n_2\rangle$ arise from the same line. There are three cases: (1) $\Gamma(|n_1\rangle) = \Gamma(|n_2\rangle)$, (2) $\Gamma(|n_1\rangle) = A_1$, $\Gamma(|n_2\rangle) = A_2$ (or vice versa), and (3) $\Gamma(|n_1\rangle) = B_1$, $\Gamma(|n_2\rangle) = B_2$ (or vice versa). In all C_{nv} groups, $A_1 \times A_2$ and $B_1 \times B_2$ do not contain E_1.[22] Thus, $\langle n_1|\hat{\mathbf{x}}\cdot\mathbf{r}|n_2\rangle = 0$ for cases 2 and 3. If n is even, the direct product of an irreducible representation with itself never contains E_1, so the matrix element is zero for case 1 as well. However, if n is odd, $E_{\frac{n-1}{2}} \times E_{\frac{n-1}{2}} \ni E_1$, while all other such products do not contain E_1. This means that $\langle n_1|\hat{\mathbf{x}}\cdot\mathbf{r}|n_2\rangle$ can be nonzero only if $|n_1\rangle$ and $|n_2\rangle$ arise from the line farthest from Γ in odd-n tubes.

We now turn to chiral tubes. The space groups of these tubes are nonsymmorphic. However, factor groups that are analogous to the above point groups can be constructed from powers of screw operations, i.e., rotations about z followed by translations along z. This was done recently by Jishi *et al.*[23] for all chiral tubes. They showed that each chiral tube has a factor group consisting of powers of a single screw operation. The factor groups are all isomorphic to the point groups C_n with n even. The irreducible representations are $A, B, E_1, E_2, ..., E_{\frac{n}{2}-1}$. A is the symmetric representation, and x, y transform as E_1. Again, we may use Eq. (A2) to carry out the analysis.

Just as for nonchiral tubes, states that arise from particular lines transform like particular irreducible representations of the factor group. The line intersecting the Γ point is associated with A, the farthest lines with B, and the others with $E_1, E_2, ...$, etc. For these groups, the direct product of an irreducible representation with itself never contains E_1. Thus, $\langle n_1|\hat{\mathbf{x}}\cdot\mathbf{r}|n_2\rangle$ is always zero if $|n_1\rangle$ and $|n_2\rangle$ arise from the same line. This is true for all chiral tubes.

[1] S.L. Ren *et al.*, Appl. Phys. Lett. **59**, 2678 (1991).
[2] G.F. Bertsch, A. Bulgac, D. Tomanek, and Y. Wang, Phys. Rev. Lett. **67**, 2690 (1991).
[3] O. Gunnarson, D. Rainer, and G. Zwicknagl, Int. J. Mod. Phys. B **6**, 3993 (1992).
[4] E. Westin and A. Rosen, Int. J. Mod. Phys. B **6**, 3893 (1992).
[5] B. Shanker and J. Applequist, J. Phys. Chem. **98**, 6486 (1994).
[6] S. Iijima, Nature (London) **354**, 56 (1991).
[7] S. Iijima and T. Ichihashi, Nature (London) **363**, 603 (1993); D.S. Bethune *et al.*, *ibid.* **363**, 605 (1993).
[8] M.F. Lin and K. W.-K. Shung, Phys. Rev. B **47**, 6617 (1993); P. Longe and S.M. Bose, *ibid.* **48**, 18 239 (1993).
[9] N. Hamada, S. Sawada, and A. Oshiyama, Phys. Rev. Lett. **68**, 1579 (1992).
[10] R. Saito, M. Fujita, G. Dresselhaus, and M.S. Dresselhaus, Appl. Phys. Lett. **60**, 2204 (1992).
[11] B. Koopmans, Ph.D. thesis, University of Groningen, 1993.
[12] H. Ehrenreich and M.H. Cohen, Phys. Rev. **115**, 786 (1959).
[13] J.C. Slater and G.F. Koster, Phys. Rev. **94**, 1498 (1954).
[14] D. Tomanek and S.G. Louie, Phys. Rev. B **37**, 8327 (1988).
[15] X. Blase, L.X. Benedict, E.L. Shirley, and S.G. Louie, Phys. Rev. Lett. **72**, 1878 (1994).
[16] M.R. Pederson and A.A. Quong, Phys. Rev. B **46**, 13 584 (1992).
[17] M.S. Hybertson and S.G. Louie, Phys. Rev. B **35**, 5585 (1987); **35**, 5602 (1987).
[18] L.D. Landau and E.M. Lifshitz, *Electrodynamics of Continuous Media* (Pergamon Press, Oxford, 1960).
[19] In order to check the internal consistency of the calculation, we calculated α_{0xx} of some of the smaller tubes with $\hat{\mathbf{x}}$ in different directions. The answer was always independent of the chosen direction.
[20] J.M. Ziman, *Principles of the Theory of Solids* (Cambridge University Press, Cambridge, 1972).
[21] J.W. Mintmire, B.I. Dunlap, and C.T. White, Phys. Rev. Lett. **68**, 631 (1992).
[22] D.C. Harris and M.D. Bertolucci, *Symmetry and Spectroscopy* (Dover, New York, 1989).
[23] R.A. Jishi, M.S. Dresselhaus, and G. Dresselhaus, Phys. Rev. B **47**, 16 671 (1993).